Acta Pharmaceutica Sinica B 2021;11(5):1341−1354

Chinese Pharmaceutical Association
Institute of Materia Medica, Chinese Academy of Medical Sciences

Acta Pharmaceutica Sinica B

www.elsevier.com/locate/apsb
www.sciencedirect.com

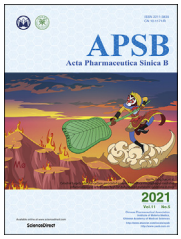

ORIGINAL ARTICLE

Escape from abluminal LRP1-mediated clearance for boosted nanoparticle brain delivery and brain metastasis treatment

Naveed Ullah Khan[a], Jiang Ni[a,b], Xiufeng Ju[a], Tongtong Miao[a], Haiyan Chen[a], Liang Han[a,*]

[a]*Jiangsu Key Laboratory of Neuropsychiatric Diseases Research and College of Pharmaceutical Sciences, Soochow University, Suzhou 215123, China*
[b]*Department of Pharmacy, Affiliated Hospital of Jiangnan University, Wuxi 214000, China*

Received 11 July 2020; received in revised form 14 September 2020; accepted 23 September 2020

KEY WORDS

Breast cancer brain metastases;
Blood–brain barrier;
Amyloid beta;
Abluminal LRP1;
Brain clearance;
Fusion peptide;
MMP;
Nanoparticles

Abstract Breast cancer brain metastases (BCBMs) are one of the most difficult malignancies to treat due to the intracranial location and multifocal growth. Chemotherapy and molecular targeted therapy are extremely ineffective for BCBMs due to the inept brain accumulation because of the formidable blood–brain barrier (BBB). Accumulation studies prove that low density lipoprotein receptor-related protein 1 (LRP1) is promising target for BBB transcytosis. However, as the primary clearance receptor for amyloid beta and tissue plasminogen activator, LRP1 at abluminal side of BBB can clear LRP1-targeting therapeutics. Matrix metalloproteinase-1 (MMP1) is highly enriched in metastatic niche to promote growth of BCBMs. Herein, it is reported that nanoparticles (NPs-K-s-A) tethered with MMP1-sensitive fusion peptide containing HER2-targeting K and LRP1-targeting angiopep-2 (A), can surmount the BBB and escape LRP1-mediated clearance in metastatic niche. NPs-K-s-A revealed infinitely superior brain accumulation to angiopep-2-decorated NPs-A in BCBMs bearing mice, while comparable brain accumulation in normal mice. The delivered doxorubicin and lapatinib synergistically inhibit BCBMs growth and prolongs

Abbreviations: 231Br, MDA-MB-231Br-HER2; A, angiopep-2; Aβ, amyloid beta; AUC_{0-t}, area under the curve from zero to time t; BBB, blood–brain barrier; BCBMs, breast cancer brain metastases; BMECs, brain microvascular endothelial cells; CI, combination index; CL, clearance; DMEM, Dulbecco's modified eagle medium; DMSO, dimethyl sulfoxide; DOX, doxorubicin; Fa, the fraction of tumor cells affected; FBS, fetal bovine serum; i, insensitive GDQGIAGF; K, KAAYSL; LAP, lapatinib; LRP1, low density lipoprotein receptor-related protein 1; MAL-PEG-SCM, maleimide polyethylene glycol succinimidyl carboxymethyl ester; MCM, MDA-MB-231Br-HER2 conditioned medium; MMP1, matrix metalloproteinase-1; MRT_{0-t}, mean residence time from zero to time t; NPs, nanoparticles; PLGA, poly(lactic-*co*-glycolic acid); PLGA-PLL, poly(lactic-*co*-glycolic acid)-poly(ε-carbobenzoxy-L-lysine); PLL, poly(ε-carbobenzoxy-L-lysine); PVA, polyvinyl alcohol; s, sensitive VPMS-MRGG; SDS, sodium dodecyl sulfate; $t_{1/2}$, half time; tPA, tissue plasminogen activator.

*Corresponding author. Tel./fax: +86 512 65882089.
E-mail address: hanliang@suda.edu.cn (Liang Han).

Peer review under responsibility of Chinese Pharmaceutical Association and Institute of Materia Medica, Chinese Academy of Medical Sciences.

https://doi.org/10.1016/j.apsb.2020.10.015

survival of mice bearing BCBMs. Due to the efficient BBB penetration, special and remarkable clearance escape, and facilitated therapeutic outcome, the fusion peptide-based drug delivery strategy may serve as a potential approach for clinical management of BCBMs.

1. Introduction

Nanotechnology-based strategies have been extensively investigated to promote brain targeting delivery efficiency[1−10]. Most strategies involve coupling of nanoparticles (NPs) with ligands which can bind with specific receptors on brain microvascular endothelial cells (BMECs)[1−10]. The binding enables receptor-mediated transcytosis in BMECs for penetrating through the blood–brain barrier (BBB). Low density lipoprotein receptor-related protein 1 (LRP1) is one of the very promising BBB targeting receptors due to its abundant expression on BMECs[11−14]. However, most ligand-functionalized NPs for BBB passing have <1% of injected dose reaching the brain tissue after systemic administration[15].

Amyloid beta (Aβ) has been extensively studied in the light of pathophysiology of Alzheimer's disease. Endogenous Aβ is produced by neurons and secreted into the brain interstitial fluid[16]. Indeed, Aβ may play a physiological role of mediating memory forgetting in the normal brain[17]. For normal individuals, brain homeostasis of Aβ is maintained through its clearance from brain into blood. The majority of Aβ (∼85%) is cleared by the BBB with a small percentage being cleared by bulk flow of interstitial fluid under physiological conditions[18]. LRP1 at abluminal side of BBB, is the key and primary Aβ clearance receptor[18−23]. Aβ binds LRP1 and initiates clearance transcytosis across BBB to transport Aβ from brain to blood[18]. Tissue plasminogen activator (tPA) is another LRP ligand[24]. It was reported that LRP regulates the clearance of tPA from brain[24]. We hypothesized that, NPs coupled with specific ligands of LRP1[25], may bind with abluminal LRP1 after BBB penetration and go through clearance transcytosis from brain to blood. The clearance can result in less accumulation of NPs in brain. Therefore, escape from abluminal LRP1-mediated clearance should be able to increase the accumulation of LRP1-targeting NPs in brain parenchyma. Moreover, doxorubicin (DOX) is one of the peerless treatments for cancer but single therapy is inadequate to treat BCBMs. The use of molecular-target lapatinib (LAP) as an adjuvant significantly increased anticancer effect of DOX in resistant breast cancer cells. Many studies revealed that LAP in combination with chemotherapy showed significant clinical efficacy rather than single therapy[26,27]. Being encouraged by previous studies, the treatment of BCBMs with the combinatorial regimen of DOX and LAP may be considered an effective approach and is a novel synergistic combinatorial regimen for BCBMs.

Therapeutics with highly efficient BBB penetration remain to be developed for the effective treatment of breast cancer brain metastases (BCBMs) because of the unavailability of surgical resection. By studying BCBMs derived from MDA-MB-231Br-HER2 (231Br) cells, a model that has been well characterized to recapitulate pathology of human BCBMs[28,29], it was found that the microenvironment in BCBMs is highly enriched with matrix metalloproteinase-1 (MMP1) for the local growth of BCBMs[30,31]. VPMS-MRGG is an optimized peptide for MMP1 degradation[32], and possesses superior properties, *e.g.*, faster degradation kinetics[33], to collagen-based GPQGYIAGQ and GPQGYIWGQ. Beside for brain targeting, angiopep-2 (A) was also used for targeting BCBMs based on the overexpression of LRP1[34,35]. KAAYSL peptide, with high affinity (K_d = 305 nmol/L) to the extracellular domain of HER2, can trigger specific HER2 binding and subsequent internalization[36], and possesses the potential for use as the targeting ligand for HER2-overexpressed 231Br cells (BCBMs).

Here, to escape from abluminal LRP1-mediated clearance when using LRP1 for brain targeting, and to improve brain accumulation for therapy of BCBMs, we designed a fusion peptide K-s-A by integrating HER2-targeting KAAYSL (K) with MMP1-sensitive VPMS-MRGG (s) and LRP1-targeting angiopep-2 (A) to decorate poly(lactic-*co*-glycolic acid)-poly(ε-carbobenzoxy-L-lysine) (PLGA-PLL) NPs (NPs-K-s-A, Scheme 1). Fusion peptide (K-i-A) with MMP1-insensitive GDQGIAGF (i) was used as control[37]. The synthesis of PLGA-PLL and the ligand coupling chemistry *via* maleimide polyethylene glycol succinimidyl carboxymethyl ester (MAL-PEG-SCM) were reported in our previous papers[34,38,39]. *In vitro* studies verified MDA-MB-231Br-HER2-conditioned medium (MCM) and MMP1 protein-regulated uptake and transcytosis in BMECs and targeting and growth inhibiting of BCBM cells. *In vivo* studies demonstrated NPs-K-s-A's prolonged circulation, comparable brain accumulation to NPs-A in normal mice, and exceedingly higher brain accumulation than NPs-A in BCBMs-bearing mice, and heightened therapeutic efficacy in BCBMs-bearing mice when loaded with combined DOX and LAP. At hand, we efficaciously envisioned and applied a healing slant to escape the LRP1 mediated clearance and treat brain metastases with DOX and LAP combinatorial regimen, which can be an effective therapeutic approach to treat brain metastases and other neurological diseases.

2. Materials and methods

2.1. Materials

Poly(lactic-*co*-glycolic acid) (PLGA, Cat. 719900) and poly(ε-carbobenzoxy-L-lysine) (PLL, Cat. P4510) were purchased from Sigma−Aldrich (Shanghai, China). Maleimide polyethylene glycol succinimidyl carboxymethyl ester (MAL-PEG-SCM, MW 5000) was obtained from Jenkem Technology (Beijing, China). Polyvinyl alcohol (PVA, #403) was obtained from Kuraray (Japan). Peptides were synthesized by Nanjing Peptide Biotech Ltd. (Nanjing, China). Dulbecco's modified Eagle's medium (DMEM) was purchased from Gibco (Tulsa, OK, USA). Other chemicals were purchased from Sigma−Aldrich unless otherwise specified, and were used as received.

2.2. Preparation of nanoparticles

In a typical synthesis, 100 mg PLGA-PLL in 2 mL ethyl ether containing 20 mg DOX or LAP was added dropwise to 4 mL 2.5% PVA under vortex and sonicated to form an oil/water emulsion. The emulsion was poured into a beaker containing 0.3% PVA and stirred overnight for evaporation of ethyl ether. The suspension was centrifuged at 3000 rpm (OPTIMAL-90K, BECKMAN, USA) for 10 min to remove unencapsulated aggregated drug and bigger particles. Then PLGA-PLL NPs were collected by centrifugation at 30,000 rpm (BECKMAN) for 20 min and resuspended in PBS 7.4 with 10 mg MAL-PEG-SCM. The primary amines from PLL were reacted with the succinimidyl carboxymethyl ester for 1 h at room temperature. Then PLGA-PLL-PEG NPs, also named "unmodified NPs" or "NPs" when compared with ligand-modified NPs, were purified and collected by centrifugation at 30,000 rpm (BECKMAN) for 20 min and resuspended in PBS 7.4 with ligands. The maleimide was reacted with cysteine on various ligands for 1 h at room temperature. Then modified NPs were purified and collected by centrifugation at 30,000 rpm (BECKMAN) for 20 min, resuspended in H_2O and lyophilized for storage and characterization.

For synthesis of IR780-loaded NPs, 1 mg of IR780 in 100 μL of dimethyl formamide and 200 μL of water were added dropwise to 100 mg of PLGA-PLL in 2 mL ethyl ether under vortex, to create the water/oil emulsion. Remaining procedures are similar to those mentioned above.

2.3. Physicochemical characterizations

NPs' size, appearance and morphology were examined under a transmission electron microscope (JEM-2010, JEOL, Japan). Hydrodynamic diameter and Zeta potential were determined using dynamic light scattering on a Zetasizer Nano ZS (Malvern Instruments, Co., Ltd.).

The drug loading efficiency was determined by microplate fluorescence reader (Synergy 2, Bioteck, USA) for DOX and HPLC (Agilent, 1260, USA) for LAP. *In vitro* release of DOX and LAP was performed in PBS 7.4 or 5.0 with 0.5% sodium dodecyl sulfate (SDS) using dialysis method.

2.4. Cell culture

Mouse BMECs bEND.3 cells were purchased from ATCC. 231Br cells were kindly provided by Dr. Patricia Steeg at the National Cancer Institute, USA. bEND.3 cells and 231Br cells were grown in DMEM medium supplemented with 10% fetal bovine serum (FBS), 100 units/mL penicillin, and 100 μg/mL streptomycin in a 37 °C incubator containing 5% CO_2.

2.5. In vitro uptake in BMECs

To explore if fusion peptides (K-s-A and K-i-A) can boost uptake in BMECs, bEND.3 cells were treated with IR780-loaded various NPs at 1.8 μg/mL IR780 for 2 h. The treated cells were lysed by radio immunoprecipitation assay buffer and extracted by dimethyl sulfoxide (DMSO) and the intracellular internalized IR780 was quantitatively measured using microplate reader (Bioteck) through its fluorescence at an excitation wavelength of 780 nm and an emission wavelength of 817 nm. Fluorescence was converted in μg IR780/mg cell proteins by determining the protein concentration using the BCA assay. A blank was prepared by detecting the fluorescence in untreated cells and the fluorescence/protein value was subtracted from that calculated in each sample.

2.6. ELISA for MMP1 measurement

MMP1 protein expression level in *in vitro* MCM was measured with human MMP1 ELISA Kit (MultiSciences, Hangzhou, China) according to the manufacturer's instruction. 231Br cells were grown to 60% confluence in medium with 10% FBS, washed three times with hanks, and incubated for another 48 h in medium with 0.5% FBS. Supernatants were separated, centrifuged for 5 min at 14,000×*g*, and used for protein determination and ELISA in parallel. The MMP1 amounts were calculated in ng/mL.

2.7. Effect of MMP1 on NPs-K-s-A

To examine the effect of MMP1 on uptake of NPs-K-s-A in BMECs, IR780-loaded NPs-K-s-A were pre-incubated with 7.86 ng/mL MMP1 for 0, 2 and 24 h with MMP1 specific inhibitor FN439 (1, 5 and 10 μmol/L). Then bEND.3 cells were treated with pre-incubated NPs-K-s-A at 1.8 μg/mL IR780 for 2 h.

To determine the action site of MMP1 on NPs, IR780-loaded NPs-K-s-A and NPs-K-i-A were pre-incubated with 7.86 ng/mL MMP1 with or without 1 μmol/L FN439 for 0, 2 and 24 h. Then bEND.3 cells were treated with pre-incubated NPs-K-s-A or NPs-K-i-A at 1.8 μg/mL IR780 for 2 h.

2.8. NPs-K-s-A response in MCM

For *in vitro* expression of LRP1 on bEND.3 cells by Western blotting, 1.4×10^5 bEND.3 cells were seeded in 6-well plates for overnight. Then cells were treated with either DMEM, or MCM for 24 h. Cell lysates were mixed with proper amount of SDS sample loading buffer (5×), boiled at 98 °C, centrifuged, and separated on SDS-PAGE gel. Proteins were transferred to PVDF membrane, which was briefly washed with double distilled water and further blocked with 10% non-fat milk in TBST, incubated with the indicated primary antibodies for 1−2 h at room temperature and the corresponding secondary antibodies, and washed three times with TBST on a plate shaker for 10 min after each antibody incubation. The protein bands on the membrane were visualized with Immobilon Western Chemiluminescent HRP Substrate (NCM Biotech) and images were recorded in Tanon 5200 Imaging System.

To check if MCM can act on NPs and influence uptake in BMECs, IR780-loaded NPs-K-s-A were pre-incubated in mixture of PBS and MCM at different volume ratios for 2 h. Then bEND.3 cells were treated with pre-incubated NPs-K-s-A at 1.8 μg/mL IR780 for 2 h to measure the uptake.

To ascertain MMP's role in MCM, IR780-loaded NPs-K-s-A were pre-incubated in PBS/MCM (1:9, *v*/*v*) for 2 or 24 h with broad-spectrum MMP inhibitor BB-94 (1, 5 and 10 μmol/L). Then bEND.3 cells were treated with pre-incubated NPs-K-s-A at 1.8 μg/mL IR780 for 2 h.

To determine the action sites on NPs, IR780-loaded NPs-K-s-A and NPs-K-i-A were pre-incubated in PBS/MCM (1:9, *v*/*v*) with or without 5 μmol/L BB-94 for 0, 2 and 24 h. Then bEND.3 cells were treated with pre-incubated NPs-K-s-A or NPs-K-i-A at 1.8 μg/mL IR780 for 2 h.

2.9. Confocal microscopy

To qualitatively determine the uptake and integrity of NPs-K-s-A in bEND.3 cells, FITC-labeled K-s-A was synthesized by GL Biochem (Shanghai, China) and used to synthesize DOX-loaded NPs-K-s-A. bEND.3 cells in glass bottom cell culture dish were treated with DOX-loaded NPs-K-s-A at 5 μg/mL DOX (1 mL) for 6 h and counter-stained using Hoechst 33342 (2 μg/mL) for 30 min. Then the cells were observed and imaged using confocal microscope.

2.10. In vitro BBB model study for backward BBB crossing from brain to blood

A 12-well Transwell plate with 3.0 μm of mean pore size membrane was used to establish the *in vitro* BBB model. The bEND.3 cells (1.0×10^5 cells/well) were seeded in the Transwell insert with 12 mm diameter. The transendothelial electrical resistance values were detected by a Millicell-ERS volt-ohmmeter to monitor the cell monolayer integrity during the cell culture process. When the transendothelial electrical resistance value achieved between 150 and 300 $\Omega \cdot cm^2$, DOX-loaded NPs-K-i-A and DOX-loaded NPs-K-s-A in normal bEND.3 medium or MCM at 2.7 μg/mL DOX (1 mL) were added into the upper chamber, respectively. After the cells were incubated for further 6 h, the medium in both upper and lower chambers were collected to measure the DOX fluorescence.

2.11. In vitro tumor targeting

To ascertain if cleaved peptide can facilitate uptake on BCBM cells, 231Br cells were treated with various IR780-loaded NPs at 1.8 μg/mL IR780 for 2 h. Primed NPs-K-s-A and NPs-K-i-A [pre-incubated in PBS/MCM (1:9, *v/v*) for 24 h] were added to evaluate the effect of the uncertain cleavage of the fusion peptides on targeting of BCBM cells. The intracellular internalized IR780 was quantitatively measured.

2.12. In vitro cytotoxicity and growth suppression effect in BCBM cells

To assess the cytotoxicity, 231Br cells were seeded in 96 well culture plates at 4000 cells per well and after 24 h were treated with blank NPs-K-s-A for 48 h. Cell proliferation was then quantified using the standard MTT assay.

To detect the synergistic effect between DOX and LAP, 231Br cells were treated with DOX-loaded NPs-K-s-A and LAP-loaded NPs-K-s-A at different DOX/LAP weight ratios. The dose effect data comparing the fraction of tumor cells affected (Fa) to drug doses were analyzed using the Chou–Talalay analysis. The data were analyzed using the CompuSyn software in order to determine the combination index values.

For selected weight ratio, 231Br cells were treated with COMBO of DOX and LAP in the form of free drug and NPs with different modifications for 48 h.

2.13. Animals

Female ICR mice of 20−25 g body weight and BALB/c nude mice of 18−20 g body weight were purchased from the Department of Experimental Animals, Soochow University, China and maintained under standard housing conditions. All experimental procedures were executed according to the protocols approved by Soochow University Animal Care and Use Committee (Soochow, China).

2.14. Pharmacokinetics

For pharmacokinetics study, ICR mice were intravenously given free IR780 or various NPs at an equivalent IR780 dose of 0.75 mg/kg. Blood samples (20 μL) were obtained at 1 min, 2, 4, 8, 12, and 24 h through the tail vein and then mixed with 180 μL of DMSO to extract IR780. The whole mixture was transferred to a 96-well plate for near infrared fluorescence imaging, and the fluorescence signal intensity was quantified using Living Image 3.0 (Caliper, CA, USA) and compared with standard samples for blood concentration–time data analysis.

2.15. In vivo NPs' accumulation in normal brain and brain bearing BCBMs

To establish BCBMs model, nude mice were anesthetized and firmly secured with front paws extended above the head. About 2.5×10^5 231Br cells in 0.1 mL PBS 7.4 were injected into the left ventricle. Then mice were carefully examined and put back into cages.

Both normal ICR mice and mice bearing BCBMs were intravenously treated with IR780-loaded NPs at an equivalent IR780 dose of 0.75 mg/kg. At 24 h, animals were perfused with PBS 7.4 followed by 4% PFA. Brains were harvested, further fixed in 4% PFA for 48 h and then imaged to detect IR780 using an IVIS system. Representative images were shown. Fluorescence intensity was also quantified using Living Image 3.0 (Caliper).

2.16. Quantitative distribution of nanoparticles in normal and BCBMs bearing mice

To quantitatively measure the brain and other major organs accumulation rate, 24 h after injection with the dose of 0.75 mg/kg IR780, mice were perfused with PBS 7.4 and then minced brain and other major organs (20 mg) were infiltrated in 180 μL of DMSO to extract IR780. Detection of IR780 was conducted using the fluorescence reading methods at 780/817 nm (Bioteck).

2.17. Evaluation of therapeutic benefits

In vivo treatments in mice bearing BCBMs were started on Day 5 after the injection of 231Br cells. Injections were performed through the tail vein 2 times a week at a dose of 5 mg/kg DOX and 7.5 mg/kg LAP mouse weight per injection. Nine mice were included in each group except saline treatment (eight mice). Mice were monitored for survival until the following criteria for euthanasia was met: the mouse became lethargic or sick and unable to feed.

2.18. Statistical analysis

All data were collected at least in triplicate and reported as mean ± SD. Comparison of two conditions was evaluated by the unpaired *t*-test. One-way ANOVA analysis was performed to determine the statistical significance of treatment related changes in survival. $^*P < 0.05$, $^{**}P < 0.01$, $^{***}P < 0.001$ were considered significant.

3. Results and discussion

3.1. Physicochemical characterizations

Various peptide ligands (K, K-, A, K-i-A, and K-s-A) were designed and used to decorate NPs' surface to endow NPs with various functions, *e.g.*, HER2-and LRP1-targeting, and abluminal LRP1-escaping. The sequences of these peptide ligands and the nomenclature of various NPs were listed in (Table 1). The N-terminal cysteine was used for conjugation with maleimide. The GSG was added to avoid the effect of NPs' steric hindrance on KAAYSL's HER2 binding according to previous work[40−42].

PLGA-PLL NPs were prepared using ultrasonic emulsion solvent evaporation method and further grafted with MAL-PEG-SCM *via* the reaction of the primary amines of PLL with the succinimidyl carboxymethyl ester to expose PEG and maleimide functional terminal. Peptide ligands were conjugated *via* the reaction of the N-terminal cysteine on ligands with the maleimide on NPs' surface. Combined therapy has been extensively investigated for treatment of various types of cancer because of the remarkable synergistic effect[43−46]. In this study, cytotoxic DOX and molecular targeted LAP were separately loaded into the developed NPs for combined therapy of BCBMs. This combination was previously used in both clinical trials and nanomedicine-based studies for treating advanced and resistant breast cancer[47−50]. By dynamic light scattering, all ligand-attached DOX-loaded NPs and LAP-loaded NPs revealed comparable mean hydrodynamic diameters (Fig. 1A), which were slightly greater than unmodified NPs possibly due to the ligand decoration on NPs surface. The hydrodynamic diameter of DOX-loaded NPs-K-s-A reflected comparable Gaussian distribution to that of LAP-loaded NPs-K-s-A (Fig. 1B). For all NPs, the polydispersity indices were below 0.2 (Supporting Information Fig. S1), indicating the uniform particle distribution. All DOX-loaded NPs and LAP-loaded NPs showed nearly neutral Zeta potential (Fig. 1C). NPs-A, NPs-K-i-A and NPs-K-s-A exhibited stronger negative Zeta potential than NPs, NPs-K and NPs-K-, which may be due to the terminal angiopep-2. Under transmission electron microscope (JEOL), DOX-loaded NPs-K-s-A reflected spherical morphology with the size in the range of 43−76 nm (Fig. 1D). Suppose all NPs-K-s-A are perfect sphere and their density is 1 mg/mm^3, then the NP number for every mg freeze-dried NPs-K-s-A with 60 nm diameter was 8.84×10^{12}. The peptide K-s-A conjugated to per mg NPs-K-s-A was measured using the BCA assay with the peptide K-s-A as the standard sample and unmodified NPs as the control and was 3.43 ± 0.28 μg. By calculating, the molecular number of peptide K-s-A was 57.6 ± 4.7 per 60 nm NPs-K-s-A.

DOX was loaded into various NPs with loading efficiency of 9.33%−9.83% (Supporting Information Fig. S2), while LAP loaded with loading efficiency of 7.44%−7.68%. There was no significant difference in both DOX loading efficiency and LAP loading efficiency between different NPs. Both DOX and LAP were released from NPs in pH-controlled and slow manner (Fig. 1E and F). For DOX (Fig. 1E), the release rate at pH 5.0 (45.5% on Day 2 and 97.4% on Day 14) was slightly faster than that at pH 7.4 (33.0% on Day 2 and 72.4% on Day 14). LAP displayed similar pH-controlled release pattern to DOX (Fig. 1F). The comparable release kinetics are beneficial to the steady ratio of DOX to LAP for the synergistic therapy.

3.2. In vitro escape from abluminal LRP1-mediated clearance

IR780, a near-infrared fluorescent probe, allows for low background and efficient *in vitro* and *in vivo* detection. Considering its negligible release from solid NPs in our previous work[51], IR780 was used for characterizing both *in vitro* uptake and *in vivo* biodistribution and pharmacokinetics of various NPs. *In vitro* uptake in bEND.3 cells (mouse BMECs) was first evaluated to investigate the brain targeting effect. IR780 concentration in NPs-K and NPs-K-treated cells didn't exceed that in unmodified NPs treated cells (Fig. 2A), suggesting the absence of HER2 expression on bEND.3 cells and HER2-targeting can't trigger BBB passing and brain targeting. Compared with uncoupled NPs, NPs-A improved IR780 uptake in bEND.3 cells by 1.57-fold. It is noteworthy that NPs-K-s-A and NPs-K-i-A also induced evidently more uptake than unbound NPs in bEND.3 cells by 1.56- and 1.53-fold, respectively, which was comparable to NPs-A, indicating the potential for BBB penetration and brain targeting.

MMP1 protein expression level was 7.86 ng/mL in MCM by ELISA measuring. This result was consistent with previous data of MMP1 concentration in conditioned medium of two variants of the MDA-MB-231 cells (231BR and 231BR3)[30], both of which possess enhanced ability to form BCBMs in nude mice. Pre-incubation by MMP1 of this concentration for 2 and 24 h decreased uptake of NPs-K-s-A in bEND.3 cells by 26.2% and 28.4% (Supporting Information Fig. S3). MMP1 inhibitor FN439 reversed the decreased uptake, suggesting that the reduced uptake may be due to the removal of the brain targeting angiopep-2 by MMP1-catalyzed cleavage. MMP1 pre-treatment didn't change uptake of NPs-K-i-A in bEND.3 cells (Supporting Information Fig. S4), demonstrating the VPMS-MRGG (in K-s-A) rather than GDQGIAGF (in K-i-A) on NPs as MMP1's cleavage site. We further examined if the *in vitro* conditioned medium of 231Br (BCBMs) can regulate NPs-K-s-A's uptake in bEND.3 cells (BMECs). Western blotting analysis proved that MDA-MB-231Br-HER2 conditioned medium (MCM) didn't affect LRP1 expression on bEND.3 cells (Supporting Information Fig. S5), suggesting positive LRP1 expression on BBB under the BCBMs condition. Preclinical and clinical evidences also show high efficiency of LRP1-targeted angiopep-2 paclitaxel conjugate (ANG1005) for BBB crossing and BCBM-targeting[52,53]. In addition, to the best of our knowledge, there is no report about Aβ aggregation in BCBMs. These evidences suggest that LRP1 is very likely to be expressed on both luminal side and abluminal

Table 1 The nomenclature and surface ligand sequence of various NPs.

Name	Sequence of peptide ligands
NPs-K	CGSG-KAAYSL[a]
NPs-K-	CGSG-KAAYSL-VPMS[b]
NPs-A	CTFFYGGSRGKRNNFKTEEY[c]
NPs-K-i-A	CGSG-KAAYSL-GDQGIAGF[d]-TFFYGGSRGKRNNFKTEEY
NPs-K-s-A	CGSG-KAAYSL-VPMSMRGG[e]-TFFYGGSRGKRNNFKTEEY

[a]HER2-targeting KAAYSL.
[b]Remaining fragment of K-s-A after MMP1 cleavage.
[c]LRP1-targeting angiopep-2.
[d]MMP1-insensitive segment.
[e]MMP1-sensitive segment.

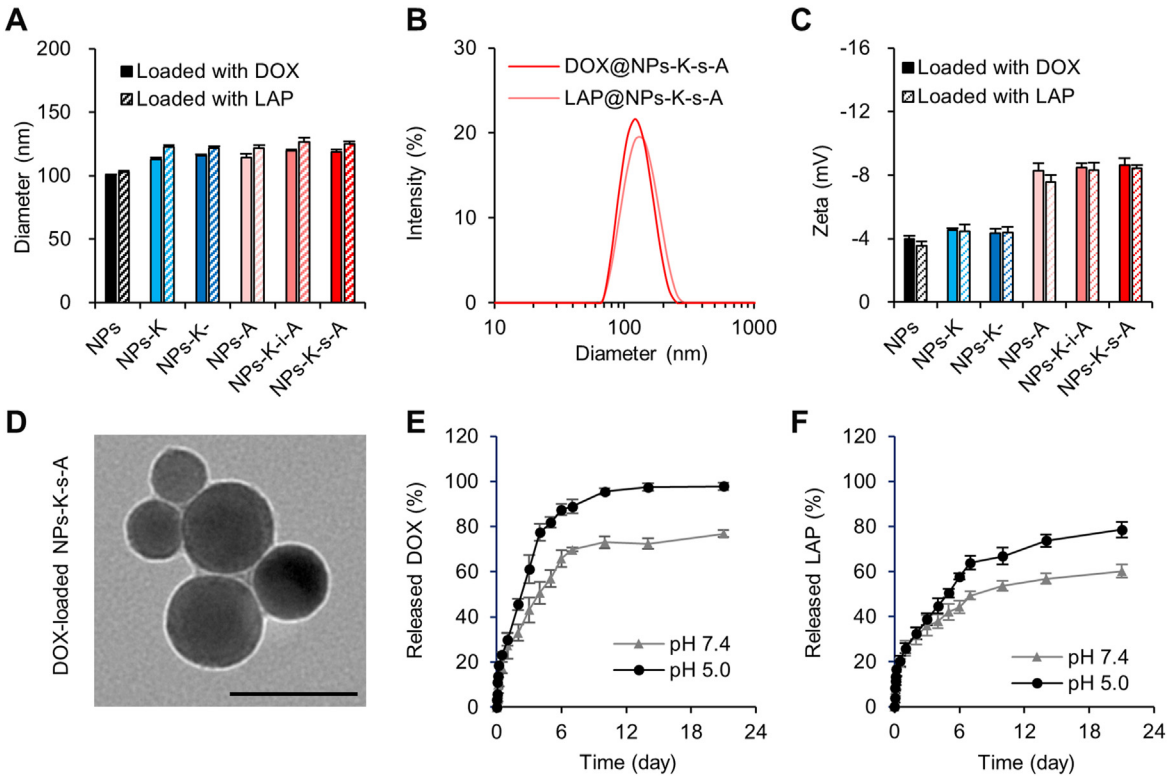

Figure 1 Characterization of nanoparticles. (A) The mean hydrodynamic size of DOX-loaded NPs and LAP-loaded NPs by dynamic light scattering. Data are presented as mean ± SD (n = 3). (B) Size distribution of DOX-loaded NPs-K-s-A and LAP-loaded NPs-K-s-A. (C) Zeta potential of DOX-loaded NPs and LAP-loaded NPs. Data are presented as mean ± SD (n = 3). (D) Representative transmission electron microscope image of DOX-loaded NPs-K-s-A. Scale bar = 100 nm. (E) and (F) *In vitro* release of DOX (E) and LAP (F) from NPs in PBS 7.4 and 5.0 containing 0.5% SDS. Data are presented as mean ± SD (n = 3).

side of BBB under the BCBMs condition. MCM pre-incubation for 2 h decreased uptake of NPs-K-s-A in bEND.3 cells by 8.9% and 12.3%, respectively (Fig. 2B), while 24 h incubation further decreased the uptake of NPs-K-s-A by 38.5% (Fig. 2C). MMP inhibitor BB-94 reversed the decreased uptake back to 92.2% and 93.5% of original uptake, respectively, suggesting the role of MMP from MCM and the possible angiopep-2 detachment by MCM caused the reduced uptake in bEND.3 cells. Pre-incubation by MCM didn't change uptake of NPs-K-i-A in bEND.3 cells (Fig. 2D).

The uptake in bEND.3 cells was also investigated qualitatively using DOX-loaded NPs with FITC-labeled K-s-A. From Fig. 2E, it can be seen that in normal medium, both DOX and FITC were efficiently internalized into bEND.3 with obvious co-localization, proving the integrity of DOX-loaded NPs-K-s-A. However, in MCM, the uptake of both DOX and FITC was dramatically reduced, which was consistent with other above data.

The backward BBB crossing from brain to blood was investigated by using Transwell filter as an *in vitro* BBB model. As shown in Fig. 2F, bEND.3 cells were cultured on a Transwell insert to form a compact monolayer. Different with most reports studying BBB crossing from blood to brain, backward BBB crossing from brain to blood was investigated in this study. So the upper chamber and the lower chamber represented brain side and blood side, respectively. The value of transendothelial electrical resistance of 150−300 Ω cm^2 indicates that the tight junction of the BBB model can be considered to be similar to that of the *in vivo* BBB[54−56]. IR780-loaded NPs-K-i-A and IR780-loaded NPs-K-s-A in normal bEND.3 medium or MCM were added into the upper chamber, respectively. After 6 h incubation, the IR780 concentration in brain side (upper chamber), endothelial cells, and blood side (lower chamber) were measured by a fluorescence spectrometer. About 23.7% and 22.0% of NPs-K-i-A (in both environments) and 25.1% of NPs-K-s-A in normal medium were cleared from brain to inside endothelium and blood. However, in MCM environments, only 6.9% of NPs-K-s-A was detected in endothelium and blood side. DOX-loaded NPs-K-i-A and DOX-loaded NPs-K-s-A were also used to investigate the backward BBB crossing. And similar results were obtained (Supporting Information Fig. S6). In the premise of existence of BCBMs, once NPs-K-s-A passes the BBB, 91.6% of the NPs-K-s-A would stay inside brain. This finding indicates that NPs-K-s-A can respond to the MCM (or microenvironment in BCBMs) to escape the clearance transcytosis from brain to blood for promoting brain accumulation, especially in regions of BCBMs.

3.3. In vitro tumor targeting and synergistic anti-tumor effect of DOX and LAP

We further investigated the *in vitro* uptake in 231Br cells (BCBMs). Compared with uncoupled NPs, NPs-K, NPs-K- and NPs-A heightened IR780 uptake (Fig. 3A). The IR780 intensity in 231Br cells treated with NPs-K, NPs-K- and NPs-A outstripped that in cells received unmodified NPs by 1.41-, 1.39-, and 1.58-fold, respectively. This result suggested that KAAYSL-driven HER2-targeting was comparable to angiopep-2-mediated LRP1-

targeting when used for BCBMs targeting and remaining VPMS after cleavage of K-s-A would not affect KAAYSL's targeting ability. Pre-incubation by MCM didn't change 231Br uptake of NPs-K-s-A (Fig. 3B), which was comparable to that of NPs-A, proving even incomplete cleavage of K-s-A would not affect BCBMs targeting because of angiopep-2's BCBMs targeting effect[34,35], besides the low interference of the left VPMS.

For *in vitro* growth inhibiting of BCBMs, blank NPs-K-s-A didn't produce any noticeable cytotoxicity even at 20 mg/mL NPs (Fig. 3C), confirming the superb safety. Then we studied the synergistic effect between DOX-loaded NPs-K-s-A and LAP-

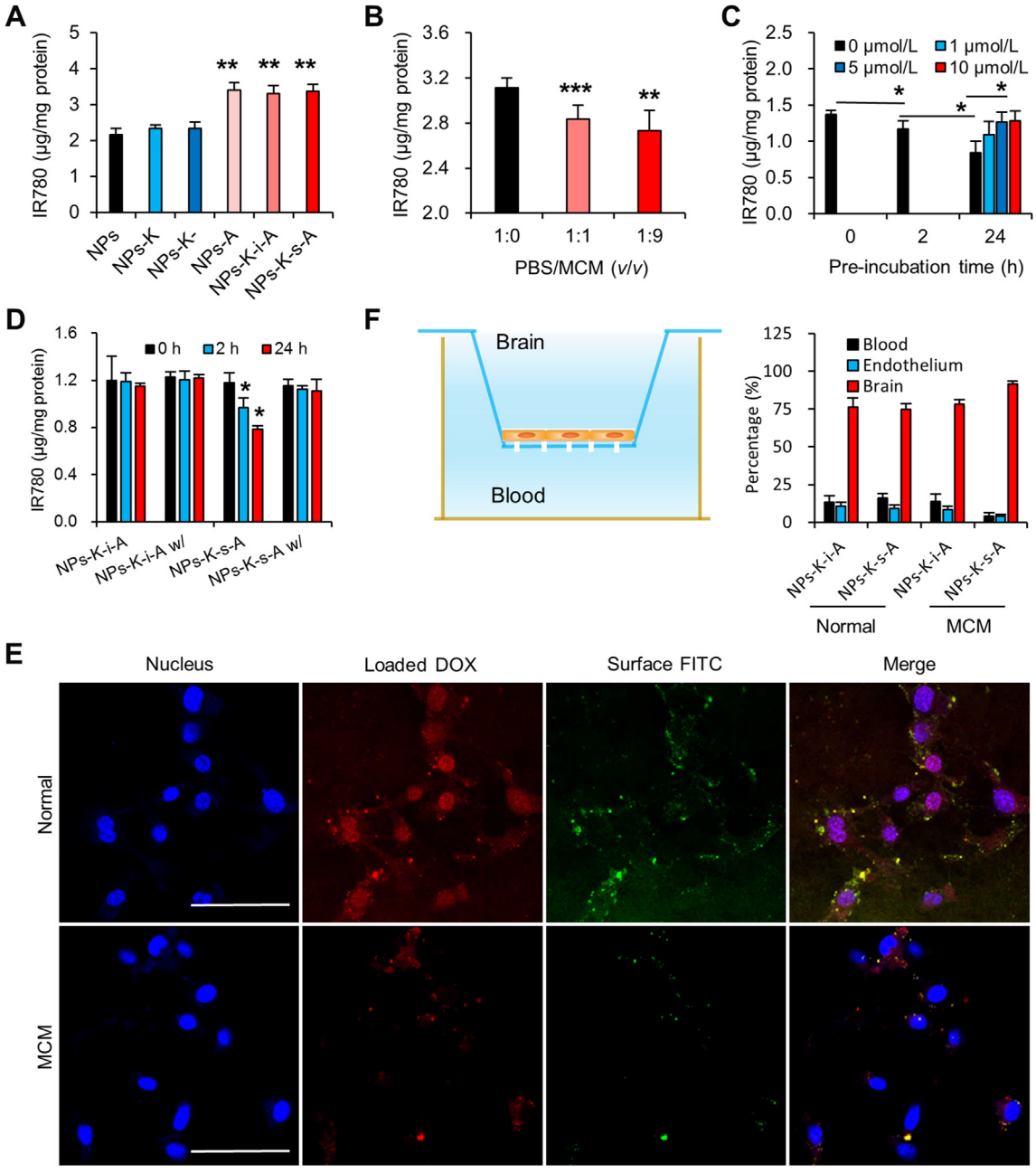

Figure 2 *In vitro* BBB transcytosis and *in vitro* escape from abluminal LRP1-mediated clearance. (A) Uptake of various NPs in normal BBB endothelial cells. Data are presented as mean ± SD ($n = 3$). (B) Uptake in bend.3 cells, NPs-K-s-A were pre-incubated in PBS/MCM mixture with different ratios for 2 h. Data are presented as mean ± SD ($n = 4$). (C) NPs-K-s-A was pre-incubated in PBS/MCM (1:9, *v/v*) for different time with different concentration MMP inhibitor BB-94. Data are presented as mean ± SD ($n = 4$). (D) NPs-K-s-A and NPs-K-i-A were pre-incubated in PBS/MCM (1:9, *v/v*) for different time with or without 5 μmol/L BB-94. Data are presented as mean ± SD ($n = 4$). (E) Qualitative uptake of DOX-loaded NPs with FITC-labeled K-s-A in normal medium or MCM in bEND.3 cells imaged using confocal microscope. Scale bar = 100 μm. (F) Left: Schematic illustration of the *in vitro* BBB model for studying backward BBB passing ability. Right: Distribution of IR780-loaded NPs-K-s-A and NPs-K-i-A in blood side, brain endothelium, and brain side. Data are presented as mean ± SD ($n = 3$). *$P < 0.05$, **$P < 0.01$, ***$P < 0.001$.

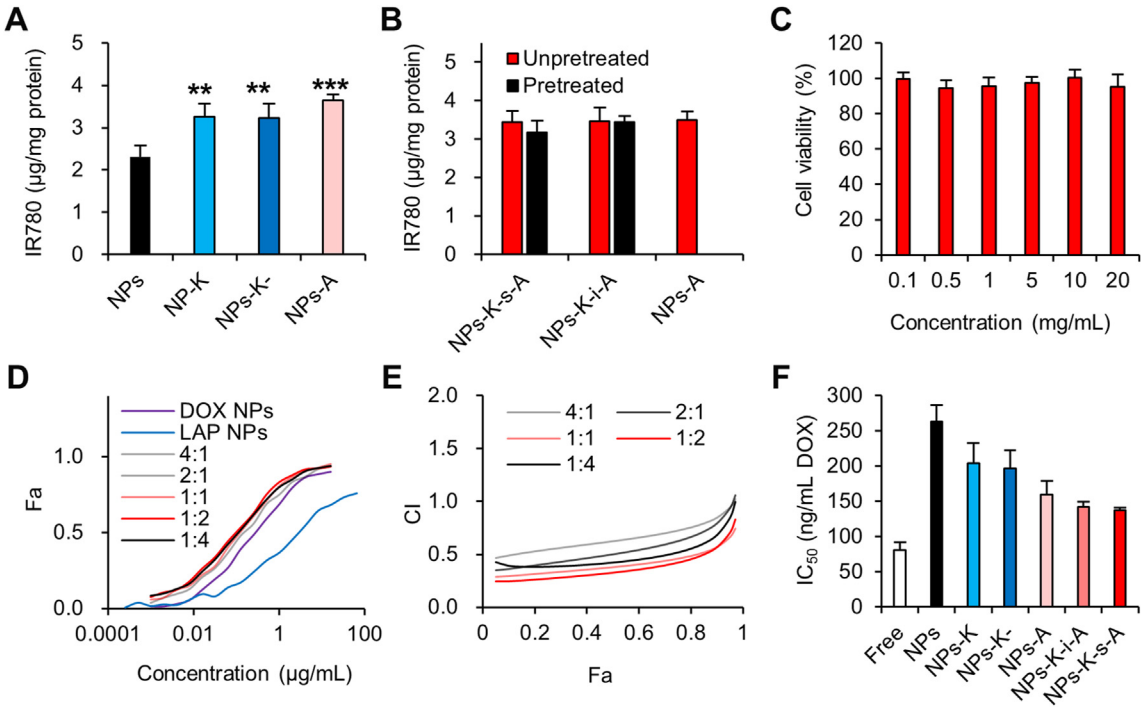

Figure 3 *In vitro* tumor targeting and synergistic anti-tumor effect of DOX and LAP combo. (A) Uptake of various IR780-loaded NPs in 231Br cells. Data are presented as mean ± SD ($n = 4$). (B) Uptake of IR780-loaded NPs in 231Br cells, which were un-pretreated or pre-incubated in PBS/MCM (1:9, *v*/*v*) for 24 h. Data are presented as mean ± SD ($n = 4$). (C) Viability of 231Br cells after treated with empty NPs-K-s-A for 48 h. Data are presented as mean ± SD ($n = 6$). (D) Dose effect curves on 231Br cells exposed to DOX-loaded NPs-K-s-A, LAP-loaded NPs-K-s-A, and COMBO NPs at different DOX/LAP weight ratios for 48 h. The fraction of 231Br cells affected (Fa) was shown. (E) The Chou−Talalay analysis of the dose effect curve in (D). Combination index (CI) values for different DOX/LAP weight ratios are provided for all Fa levels. The data were determined by the Chou−Talalay analysis model using Fa levels for actual doses. (F) IC_{50} values of different COMBO formulations (DOX/LAP = 1:1.5) on 231Br cells after incubation for 48 h. Data are presented as mean ± SD ($n = 3$). $^{**}P < 0.01$, $^{***}P < 0.001$.

loaded NPs-K-s-A. All NPs COMBO with different DOX/LAP weight ratios were more effective than DOX NPs alone and LAP NPs alone (Fig. 3D), suggesting synergy between DOX and LAP. As LAP NPs gradually added, the COMBO IC_{50} in form of DOX gradually decreased from 273 ng/mL without LAP NPs to 211–116 ng/mL (for DOX/LAP ratios of 4:1 to 1:2) and achieved the lowest point of 107 ng/mL at the ratio of 1:4. The synergy of DOX-loaded NPs-K-s-A and LAP-loaded NPs-K-s-A combination was analyzed and quantified by CompuSyn using the Chou–Talalay method[57]. The experimental and theoretical combination index (CI) values were shown in Fig. 3E. The CI < 1, >1, and = 1 indicate synergism, antagonism, and additive effect, respectively. Most concentrations in all ratios exhibited the CI values < 1, indicating synergy between DOX-loaded NPs-K-s-A and LAP-loaded NPs-K-s-A. More importantly, the lower the CI value, the stronger the synergistic effect. The CI values at ratios of 1:1 and 1:2 were comparable and below those at other ratios, demonstrating the strongest synergistic effect of DOX-loaded NPs-K-s-A and LAP-loaded NPs-K-s-A between the DOX/LAP weight ratios of 1:1 and 1:2. Given the strongest synergistic effect, the COMBO with the DOX/LAP weight ratio of 1:1.5 was selected and used for following experiments. We finally compared the cytotoxicity of different COMBO-loaded formulations to 231Br cells. All NPs revealed higher IC_{50} values than free COMBO (Fig. 3F), which may be due to the controlled drug release kinetics (Fig. 1E and F). NPs-A, NPs-K-i-A and NPs-K-s-A loaded with the COMBO displayed comparable IC_{50} values with their growth inhibiting efficiency stronger than unbound NPs, validating the comparable BCBMs targeting efficiency of KAAYSL after cleavage and angiopep-2 before cleavage. The slightly higher IC_{50} of NPs-K over NPs-A, NPs-K-i-A and NPs-K-s-A can be ascribed to the slightly lower uptake of NPs-K in 231Br cells (Fig. 3A), suggesting the slightly higher targeting efficiency of angiopep-2 over KAAYSL.

3.4. In vivo brain targeting and escape from abluminal LRP1-mediated clearance

The pharmacokinetics studies were performed to explore the blood circulation of NPs-K-s-A. NPs-K-s-A displayed different blood behavior from free IR780 (Fig. 4A), which was eliminated faster. The obtained pharmacokinetic parameters in Table 2 revealed that, NPs-K-s-A exhibited relatively sustained clearance from blood with statistically exceedingly greater area under the curve from 0 to time *t* (AUC_{0-t}), longer mean residence time from 0 to time *t* (MRT_{0-t}) and half life time ($t_{1/2}$), and lower clearance (CL). The results confirmed NPs-K-s-A's prolonged blood circulation, which is beneficial to the BBB passing. In addition, all NPs (unmodified NPs, NPs-A, NPs-K-i-A, and NPs-K-s-A) displayed similar plasma concentrations−time profiles with the difference of the pharmacokinetic parameters (AUC_{0-t}, MRT_{0-t}, $t_{1/2}$, CL) statistically insignificant between any two kinds of NPs.

Next, we determined the brain accumulation of various IR780-loaded NPs in both normal mice and mice bearing BCBMs to

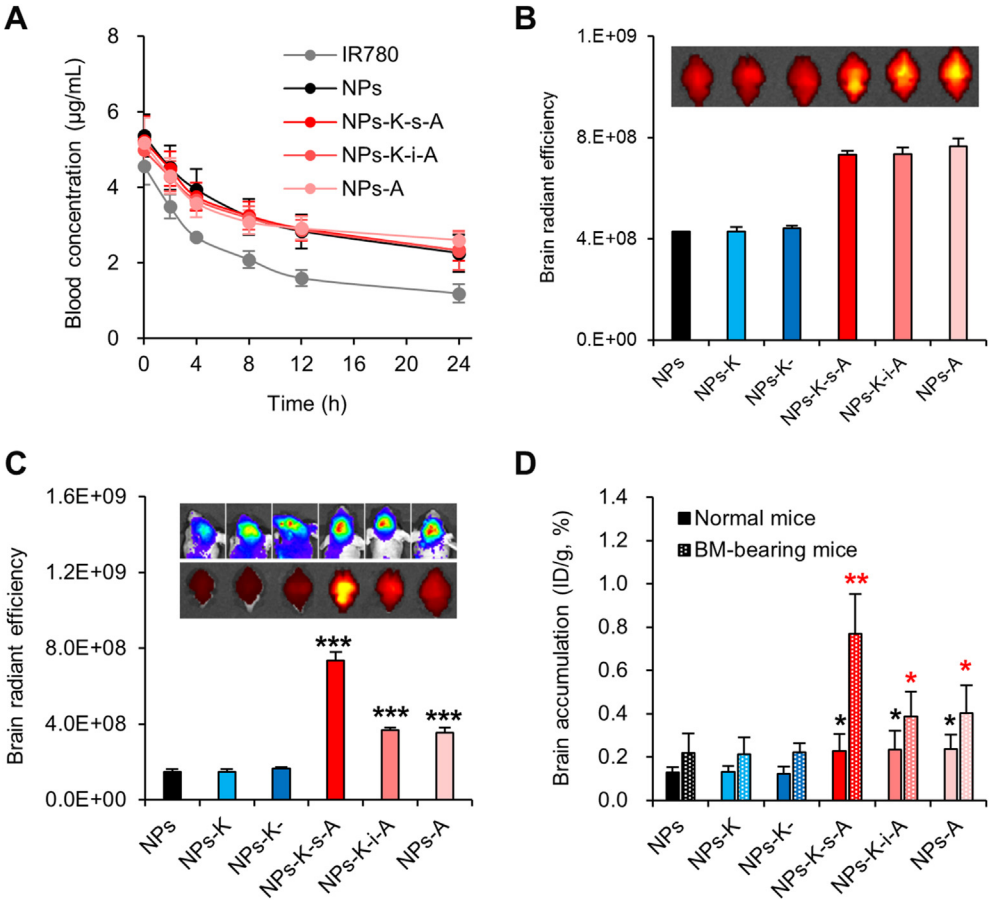

Figure 4 *In vivo* brain accumulation and escape from abluminal LRP1-mediated clearance. Mice were intravenously injected with various NPs at a dosage of 0.75 mg IR780/kg. (A) The plasma concentrations−time profiles in normal mice. Data are presented as mean ± SD ($n = 5$). (B and C) IR780 signals in excised brains from normal mice (B) and BCBMs-bearing mice (C) at 24 h after injection were determined using IVIS imaging system. Bioluminescence signal as upper image in (C) indicates BCBMs. Fluorescence intensity was quantified using Living Image 3.0. Data are presented as mean ± SD ($n = 3$). (D) Quantitative brain accumulation (ID/g, %) in normal and BCBMs-bearing mice was measured by extracted IR780. Data are presented as mean ± SD ($n = 5$ for normal mice and $n = 6$ for BCBMs-bearing mice). *$P < 0.05$, **$P < 0.01$, ***$P < 0.001$ *versus* NPs-K-s-A in (C) and *versus* NPs in (D).

assess if the BCBMs can specially strengthen NPs-K-s-A's brain accumulation. In normal mice, HER2-targeting NPs-K and NPs-K- didn't appear any signal increase in brain over unmodified NPs, suggesting HER2-targeting can't be used to trigger BBB penetration and brain accumulation (Fig. 4B). LRP1-targeting NPs-A showed enhanced signal intensity in brain by 1.90-fold compared with unbound NPs. NPs-K-s-A and NPs-K-i-A also induced apparent IR780 distribution in brain beyond uncoupled NPs by 1.81- and 1.82-fold, verifying that terminal angiopep-2 of fusion peptides (K-s-A and K-i-A) can drive LRP1-targeting for BBB crossing. There was no difference of brain signal intensity between NPs-K-s-A, NPs-K-i-A and NPs-A. We then studied if BCBMs (with MMP1 in microenvironments) can change the brain accumulation behavior of various NPs. The representative luminescence images indicated negligible size difference of BCBMs between various groups (Fig. 4C). Accumulation of NPs-K and NPs-K- in BCBMs-bearing brain was comparable to that of unbound NPs, implying that HER2-targeting alone can't play its function of BCBMs targeting because of the intact BBB surrounding BCBMs. Compared with unmodified NPs, NPs-A raised

Table 2 Pharmacokinetic parameters of NPs-K-s-A in normal ICR mice.[a]

Group	AUC_{0-t} (μg·h/mL)	MRT_{0-t} (h)	CL (mL/h/kg)	$t_{1/2}$ (h)
Free	49.07 ± 2.17	11.51 ± 1.25	0.0153 ± 0.0006	7.98 ± 0.86
NPs	143.38 ± 19.7*	28.13 ± 3.91**	0.0053 ± 0.0007***	19.51 ± 2.71**
NPs-K-s-A	139.00 ± 3.29***	30.62 ± 3.60**	0.0054 ± 0.0001***	21.22 ± 2.50**
NPs-K-i-A	144.85 ± 21.47**	32.35 ± 3.21**	0.0050 ± 0.0007***	22.43 ± 2.23**
NPs-A	155.90 ± 9.57**	36.19 ± 3.47**	0.0049 ± 0.0002***	25.09 ± 2.40**

[a]Data are presented as mean ± SD ($n = 5$). *$P < 0.05$, **$P < 0.01$, ***$P < 0.001$ *versus* free groups.

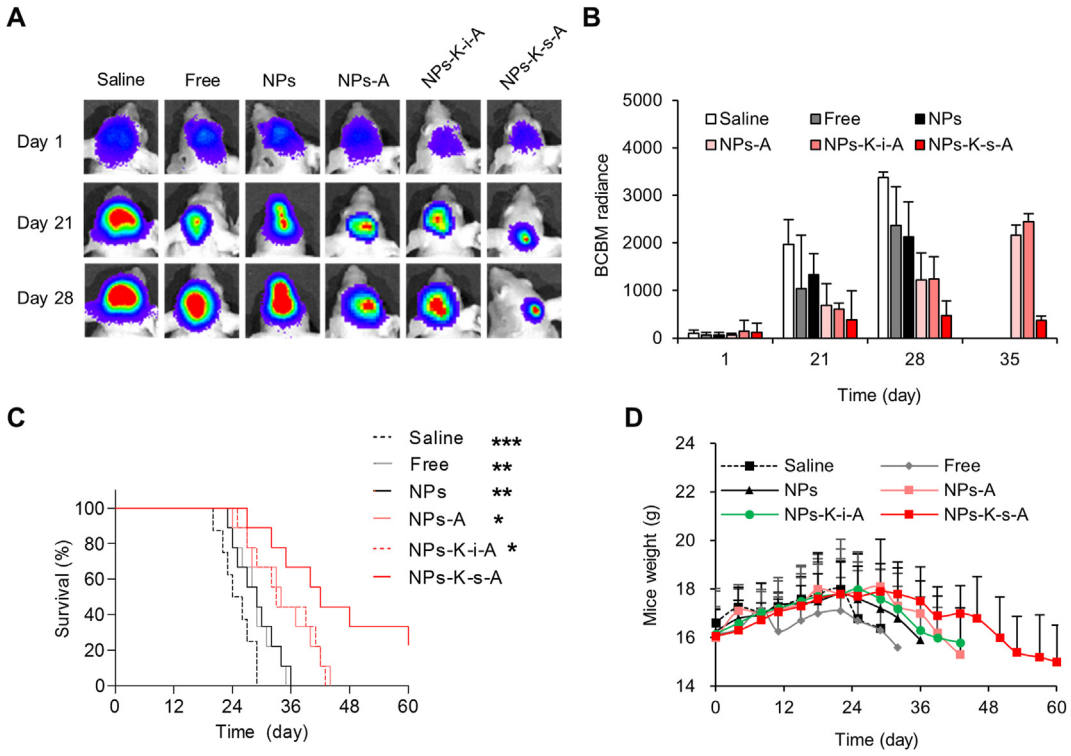

Figure 5 *In vivo* therapeutic efficacy. (A) Representative images of the development of BCBMs in the brain imaged by IVIS in mice received the indicated treatment. (B) The bioluminescence intensity of BCBMs was quantified using Living Image 3.0. (C) Kaplan−Meier survival curves of BCBMs-bearing mice received the indicated treatments. (D) Change of body weight of mice received the indicated treatments with time. Data are presented as mean ± SD ($n = 8$ for saline treatment and $n = 9$ for other treatments). *$P < 0.05$, **$P < 0.01$, ***$P < 0.001$ *versus* NPs-K-s-A.

brain accumulation by 2.39-fold. The higher brain accumulation efficiency of NPs-A in BCBMs-bearing brain (2.39-fold increase) than in normal mice (1.90-fold increase) can be ascribed to angiopep-2-mediated special uptake in BCBM cells. With insensitive fusion peptide at surface, NPs-K-i-A induced NPs-A-comparable IR780 intensity in brain (2.48-fold). However, NPs-K-s-A with MMP1 sensitivity induced astonishing brain accumulation of IR780 (4.94-fold), which was higher than NPs-A and NPs-K-i-A, which can be explained by the escape from abluminal LRP1-mediated clearance from brain to blood *via* MMP1-catalyzed angiopep-2 removal. The measured brain accumulation in form of %ID/g by extracting IR780 also showed same findings (Fig. 4D). LRP1 is implicated in brain clearance of many macromolecules including Aβ and protease/α2-macroglobulin complexes[58]. About 85% of Aβ is cleared by LRP1 at abluminal side of BBB[18]. It has been reported that the clearance of reconstituted high density lipoprotein NPs and poly(ethylene glycol)-*b*-poly(lactic acid) NPs was significantly declined in APP/PS1 mice[59] (Alzheimer's disease model with LRP1 down-regulation in brain[60]). These evidences suggest that it is very likely that LRP1 at abluminal side of BBB, to a great extent, contributes to NPs' brain clearance. However, the exact extent of NPs' brain clearance by LRP1 at abluminal side of BBB needs more in-depth studies, which may involve transgenic mice or pharmacological inhibition approaches. BMECs provide a transcellular barrier by virtue of their small number of endocytotic vesicles, leading to slower transcytosis rate at brain endothelium than that at peripheral vasculature[61,62]. Previously we reported simvastatin-induced LRP1 up-regulation to surmount the low transcytosis of BBB[34]. The decoration with fusion peptide K-s-A also holds the potential for combining with the simvastatin-induced LRP1 up-regulation for further improvement of brain delivery efficacy. Other surface properties including size and Zeta potential can be optimized. In addition, biomimetic delivery platforms with excellent *in vivo* behaviors[63−65], can be functionalized with the fusion peptide K-s-A for further boost. For peripheral organs, all kinds of NPs distributed in the order of liver, spleen, kidney, lung, and heart (Supporting Information Figs. S7 and S8). There was no significant difference between mice given different injections and between normal mice and BCBMs-bearing mice.

3.5. *Evaluation of therapeutic benefits*

By fruitful escape from abluminal LRP1-mediated clearance and improved accumulation in brain, especially in regions of BCBMs, NPs-K-s-A showed the great potential for targeted delivery of therapeutics for treatment of BCBMs. We further explored the feasibility of using the DOX/LAP COMBO delivered by NPs-K-s-A to treat established BCBMs on mice. Bioluminescence imaging of the stably transfected luciferase on 231Br cells was performed to screen successful animal models and also the growth of BCBMs. From the representative bioluminescence images, brain showed evident enrichment of bioluminescent signal on Day 1 (Supporting Information Fig. S9). Animals with comparable brain signal were chosen (Fig. 5A), and randomly grouped for various treatments. Both BCBMs growth and mouse survival were monitored. Systemic treatment of COMBO delivered by NPs-K-s-A observably inhibited the BCBMs growth with the signal 19.5%, 37.1%, 28.5%, 55.5%, and 63.2% that of saline, free COMBO,

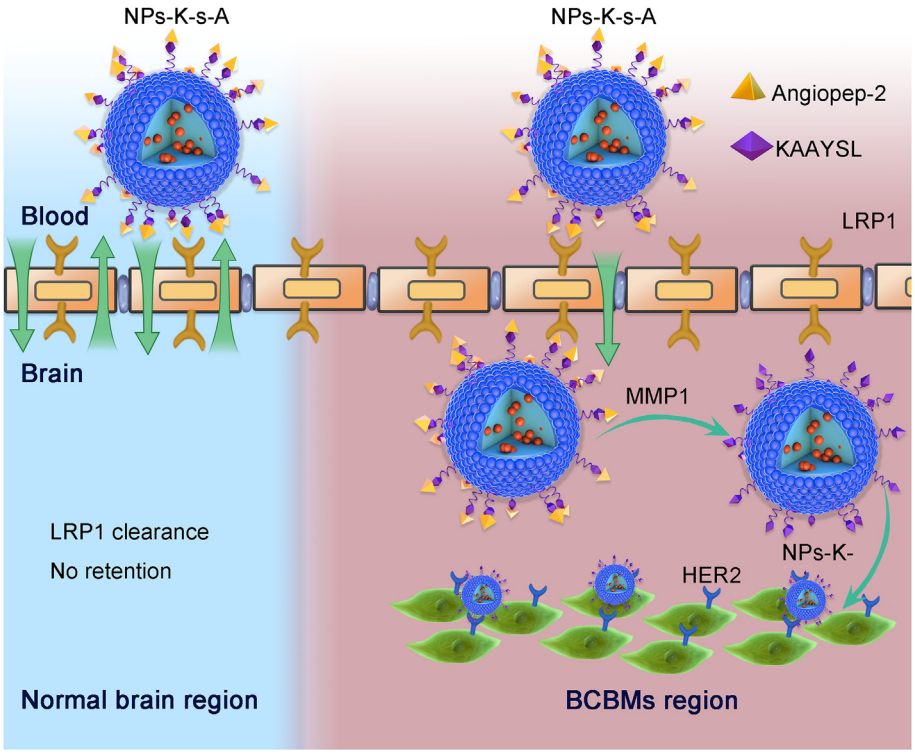

Scheme 1 NPs-K-s-A penetrate through BBB and escape abluminal LRP1-mediated clearance from BCBMs-associated BBB through separating LRP1-targeting angiopep2 *via* MMP1-triggered cleavage in metastatic niche for augmented accumulation in BCBMs-bearing brain and subsequent BCBMs-targeting.

unbound NPs, NPs-A and NPs-K-i-A-treated mice, respectively, on Day 21 after intracardiac injection of the 231Br cells (Fig. 5B). On Day 28, the relative growth by the bioluminescent signal intensity ratio further decreased to 14.1%, 20.1%, 22.3%, 39.1%, and 38.0% (Fig. 5B). Because of the death of most mice treated with saline, free COMBO and unbound NPs between Days 28−35, the relative growth of BCBMs in NPs-K-s-A-treated mice was measured against NPs-A and NPs-K-i-A on Day 35 and was 16.9% and 14.9%, respectively. The insignificant difference in tumor signal intensity between mice treated with saline and free COMBO indicated the low penetration of free drug[66]. The inefficiency of unmodified NPs substantiated the fact that the BBB disruption degree in BCBMs is insufficient for drug delivery to brain in a pharmacologically significant quantity[66,67]. The combo delivered by NPs-A or NPs-K-i-A showed moderate growth inhibiting effect. The stronger inhibiting effect of NPs-K-s-A than NPs-A or NPs-K-i-A confirmed improved delivery of therapeutics to brain or regions of BCBMs, which may be due to the efficient escape from abluminal LRP1-mediated clearance.

With the obvious growth inhibiting effect, the COMBO delivered by NPs-K-s-A markedly prolonged the survival of mice bearing BCBMs. The development of an efficient drug delivery system, which is capable of passing through the BBB and evading the clearing transcytosis, is critical for the improved treatment of BCBMs, especially for the early co-opted micrometastases. The median survival of mice treated with NPs-K-s-A was up to 42 days, which was distinctly longer than that of mice treated with saline (25 days), free COMBO (29 days), unmodified NPs (29 days), NPs-A (34 days), NPs-K-i-A (33 days) (Fig. 5C). In addition, compared with mice given other treatments, mice treated with COMBO-loaded NPs-K-s-A showed the latest loss of body weight, suggesting the modest intervention of progress of BCBMs (Fig. 5D). For *in vivo* systemic toxicity, indirectly, no visible loss of body weight was observed during the treatment period and before the worsening of BCBMs except free COMBO (Fig. 5D). All NPs treatment expressed the stable tendency of body weight, comparable to saline treatment.

4. Conclusions

There is an imperative clinical demand to design effective systemic therapies for BCBMs because of the gradually increasing incidence and the poor prognosis under present insufficient surgical treatment and radiation therapy. Most functionalized delivery platforms based on various BBB penetration strategies still have extremely low brain accumulation after systemic administration. The abluminal LRP1-mediated clearance transcytosis from brain to blood may contribute to the low brain delivery efficiency when using LRP1 for brain targeting. In this study, we proposed an innovative nanotechnology-based strategy to escape from abluminal LRP1-mediated clearance to improve brain accumulation for therapy of BCBMs. The approach was implemented by engineering NPs modified with MMP1-cleavable fusion peptide K-s-A. The developed NPs can cross the BBB through the luminal LRP1, respond to the MMP1 in microenvironment of BCBMs to detach the targeting angiopep-2 for evading the abluminal LRP1-mediated clearance, and then target BCBMs *via* the remaining targeting peptide KAAYSL, leading to facilitated brain accumulation and BCBMs targeting. The results indicate that the NPs-K-s-A may be a promising strategy for efficient brain targeting and combined therapy of BCBMs. In addition, fluorescence

dyes will be selected and design concept will be optimized to construct fluorescence resonance energy transfer system to further evaluate the disassociation of angiopep-2 from NPs-K-s-A. The capacity in reducing brain clearance can be further studied by evaluating brain retention after intraparenchymal administration[59]. Notably, the extent of the clearance of LRP1-targeting NPs by abluminal LRP1 needs future further in-depth studies, which may involve transgenic mice or pharmacological inhibition approaches. In summary, due to the high efficiency in accumulation in brain, especially in regions of BCBMs, targeting BCBMs, and the construction from safe materials with minimal toxicity, NPs-K-s-A can be potentially translated as the predominant treatment for patients unsuitable for surgical resection (most patients with BCBMs) and the adjuvant therapy to the resection cavity bed after operation to guarantee maximum removal of cancer.

Acknowledgments

This work was supported by the National Natural Science Foundation of China (Nos. 81703428 and 81973254), the Natural Science Foundation of Jiangsu Province (No. BK20191421, China), the Suzhou Science and Technology Development Project (No. SYS2019033, China), and the Priority Academic Program Development of the Jiangsu Higher Education Institutes (PAPD, China).

Author contributions

Liang Han designed the research, obtained the funding and superintended the whole study. Naveed Ullah Khan and Jiang Ni carried out the experiments and performed data analysis. Xiufeng Ju, Tongtong Miao, and Haiyan Chen participated part of the experiments. Liang Han wrote the manuscript. Naveed Ullah Khan and Jiang Ni revised the manuscript. All of the authors have read and approved the final manuscript.

Conflicts of interest

The authors have no conflicts of interest to declare.

Appendix A. Supporting information

Supporting data to this article can be found online at https://doi.org/10.1016/j.apsb.2020.10.015.

References

1. Wei L, Guo XY, Yang T, Yu MZ, Chen DW, Wang JC. Brain tumor-targeted therapy by systemic delivery of siRNA with transferrin receptor-mediated core-shell nanoparticles. *Int J Pharm* 2016;**510**:394–405.
2. Zhu YQ, Jiang Y, Meng FH, Deng C, Cheng R, Zhang J, et al. Highly efficacious and specific anti-glioma chemotherapy by tandem nanomicelles co-functionalized with brain tumor-targeting and cell-penetrating peptides. *J Control Release* 2018;**278**:1–8.
3. Li JF, Zhou L, Ye DY, Huang SX, Shao K, Huang RQ, et al. Choline-derivate-modified nanoparticles for brain-targeting gene delivery. *Adv Mater* 2011;**23**:4516–20.
4. An S, Kuang YY, Shen T, Li JF, Ma HJ, Guo YB, et al. Brain-targeting delivery for RNAi neuroprotection against cerebral ischemia reperfusion injury. *Biomaterials* 2013;**34**:8949–59.
5. Shao K, Zhang Y, Ding N, Huang SX, Wu JQ, Li JF, et al. Functionalized nanoscale micelles with brain targeting ability and intercellular microenvironment biosensitivity for anti-intracranial infection applications. *Adv Healthc Mater* 2015;**4**:291–300.
6. Liu Y, An S, Li JF, Kuang YY, He X, Guo YB, et al. Brain-targeted co-delivery of therapeutic gene and peptide by multifunctional nanoparticles in Alzheimer's disease mice. *Biomaterials* 2016;**80**:33–45.
7. Li C, Wang JC, Wang YG, Gao HL, Wei G, Huang YZ, et al. Recent progress in drug delivery. *Acta Pharm Sin B* 2019;**9**:1145–62.
8. Gao HL. Progress and perspectives on targeting nanoparticles for brain drug delivery. *Acta Pharm Sin B* 2016;**6**:268–86.
9. Gao HL. Perspectives on dual targeting delivery systems for brain tumors. *J Neuroimmune Pharmacol* 2017;**12**:6–16.
10. Ruan SB, Xie R, Qin L, Yu MN, Xiao W, Hu C, et al. Aggregable nanoparticles-enabled chemotherapy and autophagy inhibition combined with anti-PD-L1 antibody for improved glioma treatment. *Nano Lett* 2019;**19**:8318–32.
11. Huang SX, Li JF, Han L, Liu SH, Ma HJ, Huang RQ, et al. Dual targeting effect of angiopep-2-modified, DNA-loaded nanoparticles for glioma. *Biomaterials* 2011;**32**:6832–8.
12. Shao K, Wu JQ, Chen ZQ, Huang SX, Li JF, Ye LY, et al. A brain-vectored angiopep-2 based polymeric micelles for the treatment of intracranial fungal infection. *Biomaterials* 2012;**33**:6898–907.
13. Huang RQ, Ma HJ, Guo YB, Liu SH, Kuang YY, Shao K, et al. Angiopep-conjugated nanoparticles for targeted long-term gene therapy of Parkinson's disease. *Pharm Res (N Y)* 2013;**30**:2549–59.
14. Ruan SB, Yuan MQ, Zhang L, Hu GL, Chen JT, Cun XL, et al. Tumor microenvironment sensitive doxorubicin delivery and release to glioma using angiopep-2 decorated gold nanoparticles. *Biomaterials* 2015;**37**:425–35.
15. Chen EM, Quijano AR, Seo YE, Jackson C, Josowitz AD, Noorbakhsh S, et al. Biodegradable PEG-poly(ω-pentadecalactone-*co*-*p*-dioxanone) nanoparticles for enhanced and sustained drug delivery to treat brain tumors. *Biomaterials* 2018;**178**:193–203.
16. Kang JE, Lim MM, Bateman RJ, Lee JJ, Smyth LP, Cirrito JR, et al. Amyloid-beta dynamics are regulated by orexin and the sleep-wake cycle. *Science* 2009;**326**:1005–7.
17. Lee S, Kim J, Choi S. Endogenous amyloid-β mediates memory forgetting in the normal brain. *Biochem Biophys Res Commun* 2018;**506**:492–7.
18. Ramanathan A, Nelson AR, Sagare AP, Zlokovic BV. Impaired vascular-mediated clearance of brain amyloid beta in Alzheimer's disease: the role, regulation and restoration of LRP1. *Front Aging Neurosci* 2015;**7**:136–48.
19. Zandl-Lang M, Fanaee-Danesh E, Sun YD, Albrecher NM, Gali CC, Cancar I, et al. Regulatory effects of simvastatin and apoJ on APP processing and amyloid-β clearance in blood–brain barrier endothelial cells. *Biochim Biophys Acta Mol Cell Biol Lipids* 2018;**1863**:40–60.
20. Andras IE, Eum SY, Huang W, Zhong Y, Hennig B, Toborek M. HIV-1-induced amyloid beta accumulation in brain endothelial cells is attenuated by simvastatin. *Mol Cell Neurosci* 2010;**43**:232–43.
21. Zlokovic BV, Yamada S, Holtzman D, Ghiso J, Frangione B. Clearance of amyloid beta-peptide from brain: transport or metabolism?. *Nat Med* 2000;**6**:718–9.
22. Zhao Z, Sagare AP, Ma QY, Halliday MR, Kong P, Kisler K, et al. Central role for PICALM in amyloid-β blood–brain barrier transcytosis and clearance. *Nat Neurosci* 2015;**18**:978–87.
23. Storck SE, Hartz AMS, Bernard J, Wolf A, Kachlmeier A, Mahringer A, et al. The concerted amyloid-beta clearance of LRP1 and ABCB1/P-gp across the blood–brain barrier is linked by PICALM. *Brain Behav Immun* 2018;**73**:21–33.

24. Krol S, Macrez R, Docagne F, Defer G, Laurent S, Rahman M, et al. Therapeutic benefits from nanoparticles: the potential significance of nanoscience in diseases with compromise to the blood–brain barrier. *Chem Rev* 2013;**113**:1877–903.
25. Ying XY, Wang Y, Liang J, Yue JX, Xu CL, Lu LN, et al. Angiopep-conjugated electro-responsive hydrogel nanoparticles: therapeutic potential for epilepsy. *Angew Chem Int Ed* 2014;**53**:12436–40.
26. Clayton AJ, Danson S, Jolly S, Ryder WDJ, Burt PA, Stewart AL, et al. Incidence of cerebral metastases in patients treated with trastuzumab for metastatic breast cancer. *Br J Cancer* 2004;**91**:639–43.
27. Kodack DP, Chung E, Yamashita H, Incio J, Duyverman AMMJ, Song Y, et al. Jain combined targeting of HER2 and VEGFR2 for effective treatment of HER2-amplified breast cancer brain metastases. *Proc Natl Acad Sci U S A* 2012;**109**:E3119–27.
28. Palmieri D, Bronder JL, Herring JM, Yoneda T, Weil RJ, Stark AM, et al. Her-2 overexpression increases the metastatic outgrowth of breast cancer cells in the brain. *Cancer Res* 2007;**67**:4190–8.
29. Yoneda T, Williams PJ, Hiraga T, Niewolna M, Nishimura R. A bone-seeking clone exhibits different biological properties from the MDA-MB-231 parental human breast cancer cells and a brain-seeking clone *in vivo* and *in vitro*. *J Bone Miner Res* 2001;**16**:1486–95.
30. Liu H, Kato Y, Erzinger SA, Kiriakova GM, Qian YZ, Palmieri D, et al. The role of MMP-1 in breast cancer growth and metastasis to the brain in a xenograft model. *BMC Canc* 2012;**12**:583.
31. Stark AM, Anuszkiewicz B, Mentlein R, Yoneda T, Mehdorn HM, Held-Feindt J. Differential expression of matrix metalloproteinases in brain- and bone-seeking clones of metastatic MDA-MB-231 breast cancer cells. *J Neuro Oncol* 2007;**81**:39–48.
32. Turk BE, Huang LL, Piro ET, Cantley LC. Determination of protease cleavage site motifs using mixture-based oriented peptide libraries. *Nat Biotechnol* 2001;**19**:661–7.
33. Patterson J, Hubbell JA. Enhanced proteolytic degradation of molecularly engineered PEG hydrogels in response to MMP-1 and MMP-2. *Biomaterials* 2010;**31**:7836–45.
34. Guo Q, Zhu QN, Miao TT, Tao J, Ju XF, Sun ZL, et al. LRP1-upregulated nanoparticles for efficiently conquering the blood–brain barrier and targetedly suppressing multifocal and infiltrative brain metastases. *J Control Release* 2019;**303**:117–29.
35. Demeule M, Currie JC, Bertrand Y, Che C, Nguyen T, Regina A, et al. Involvement of the low-density lipoprotein receptor-related protein in the transcytosis of the brain delivery vector angiopep-2. *J Neurochem* 2008;**106**:1534–44.
36. Kumar SR, Quinn TP, Deutscher SL. Evaluation of an ^{111}In-radiolabeled peptide as a targeting and imaging agent for ErbB-2 - receptor expressing breast carcinomas. *Clin Cancer Res* 2007;**13**:6070–9.
37. Lutolf MP, Raeber GP, Zisch AH, Tirelli N, Hubbell JA. Cell responsive synthetic hydrogel. *Adv Mater* 2003;**15**:888–92.
38. Han L, Cai Q, Tian DF, Kong DK, Gou XC, Chen ZM, et al. Targeted drug delivery to ischemic stroke *via* chlorotoxin-anchored, lexiscan-loaded nanoparticles. *Nanomedicine* 2016;**12**:1833–42.
39. Miao TT, Ju XF, Zhu QN, Wang YM, Guo Q, Sun T, et al. Nanoparticles surmounting blood–brain tumor barrier through transcellular and paracellular pathways to target brain metastases. *Adv Funct Mater* 2019;**29**:1900259.
40. Kawamoto M, Horibe T, Kohno M, Kawakami K. HER2-targeted hybrid peptide that blocks Her2 tyrosine kinase disintegrates cancer cell membrane and inhibits tumor growth *in vivo*. *Mol Canc Therapeut* 2013;**12**:384–93.
41. Kumar SR, Gallazzi FA, Ferdani R, Anderson CJ, Quinn TP, Deutscher SL. *In vitro* and *in vivo* evaluation of ^{64}Cu-radiolabeled KCCYSL peptides for targeting epidermal growth factor receptor-2 in breast carcinomas. *Cancer Biother Radiopharm* 2010;**25**:693–703.
42. Cai HW, Singh AN, Sun XK, Peng FY. Synthesis and characterization of Her2-NLP peptide conjugates targeting circulating breast cancer cells: cellular uptake and localization by fluorescent microscopic imaging. *J Fluoresc* 2015;**25**:113–7.
43. Chen QJ, Liu LS, Lu YF, Chen XL, Zhang YJ, Zhou WX, et al. Tumor microenvironment-triggered aggregated magnetic nanoparticles for reinforced image-guided immunogenic chemotherapy. *Adv Sci* 2019;**6**:1802134.
44. Chen XL, Zhou WX, Liang C, Shi S, Yu XJ, Chen QJ, et al. Co-delivery nanosystem targeting the deep microenvironment of pancreatic cancer. *Nano Lett* 2019;**19**:3527–34.
45. Guo Q, He X, Li C, He YQ, Peng YY, Zhang Y, et al. Dandelion-like tailorable nanoparticles for tumor microenvironment modulation. *Adv Sci* 2019;**6**:1901430.
46. Sun T, Zhang GP, Guo ZY, Chen QJ, Zhang YJ, Chu YC, et al. Co-delivery of Cu(I) chelator and chemotherapeutics as a new strategy for tumor theranostic. *J Control Release* 2020;**321**:483–96.
47. Kwon YS, Chun SY, Nam KS, Kim S. Lapatinib sensitizes quiescent MDA-MB-231 breast cancer cells to doxorubicin by inhibiting the expression of multidrug resistance-associated protein-1. *Oncol Rep* 2015;**34**:884–90.
48. Rocca A, Cecconetto L, Passardi A, Melegari E, Andreis D, Monti M, et al. Phase Ib dose-finding trial of lapatinib plus pegylated liposomal doxorubicin in advanced HER2-positive breast cancer. *Cancer Chemother Pharmacol* 2017;**79**:863–71.
49. Pircher M, Mlineritsch B, Fridrik MA, Dittrich C, Lang A, Petru E, et al. Lapatinib-plus-pegylated liposomal doxorubicin in advanced HER2-positive breast cancer following trastuzumab: a phase II trial. *Anticancer Res* 2015;**35**:517–21.
50. Wang HY, Li F, Du CA, Wang HX, Mahato RI, Huang YZ. Doxorubicin and lapatinib combination nanomedicine for treating resistant breast cancer. *Mol Pharm* 2014;**11**:2600–11.
51. Han L, Kong DK, Zheng MQ, Murikinati S, Ma C, Yuan P, et al. Increased nanoparticle delivery to brain tumors by autocatalytic priming for improved treatment and imaging. *ACS Nano* 2016;**10**:4209–18.
52. Kumthekar P, Tang SC, Brenner AJ, Kesari S, Piccioni DE, Anders C, et al. ANG1005, a brain-penetrating peptide-drug conjugate, shows activity in patients with breast cancer with leptomeningeal carcinomatosis and recurrent brain metastases. *Clin Cancer Res* 2020;**26**:2789–99.
53. Thomas FC, Taskar K, Rudraraju V, Goda S, Thorsheim HR, Gaasch JA, et al. Uptake of ANG1005, a novel paclitaxel derivative, through the blood–brain barrier into brain and experimental brain metastases of breast cancer. *Pharm Res (N Y)* 2009;**26**:2486–94.
54. He CS, Li J, Cai P, Ahmed T, Henderson JT, Foltz WD, et al. Two-step targeted hybrid nanoconstructs increase brain penetration and efficacy of the therapeutic antibody trastuzumab against brain metastasis of her2-positive breast cancer. *Adv Funct Mater* 2018;**28**:1705668.
55. Wang CX, Wu B, Wu YT, Song XY, Zhang SH, Liu ZH. Camouflaging nanoparticles with brain metastatic tumor cell membranes: a new strategy to traverse blood–brain barrier for imaging and therapy of brain tumors. *Adv Funct Mater* 2020;**30**:1909369.
56. Shen ZY, Liu T, Li Y, Lau J, Yang Z, Fan WP, et al. Fenton-reaction-acceleratable magnetic nanoparticles for ferroptosis therapy of orthotopic brain tumors. *ACS Nano* 2018;**12**:11355–65.
57. Chou TC. Drug combination studies and their synergy quantification using the chou–talalay method. *Cancer Res* 2010;**70**:440–6.
58. Strazielle N, Ghersi-Egea JF. Potential pathways for CNS drug delivery across the blood-cerebrospinal fluid barrier. *Curr Pharmaceut Des* 2016;**22**:5463–76.
59. Gu X, Song QX, Zhang Q, Huang M, Zheng MN, Chen J, et al. Clearance of two organic nanoparticles from the brain *via* the paravascular pathway. *J Control Release* 2020;**322**:31–41.
60. He YY, Ruganzu JB, Zheng QZ, Wu XY, Jin H, Peng XQ, et al. Silencing of LRP1 exacerbates inflammatory response *via* TLR4/NF-κB/MAPKs signaling pathways in APP/PS1 transgenic mice. *Mol Neurobiol* 2020;**57**:3727–43.

61. Abbott NJ, Patabendige AAK, Dolman DEM, Yusof SR, Begley DJ. Structure and function of the blood–brain barrier. *Neurobiol Dis* 2010; **37**:13−25.
62. Knowland D, Arac A, Sekiguchi KJ, Hsu M, Lutz SE, Perrino J, et al. Stepwise recruitment of transcellular and paracellular pathways underlies blood–brain barrier breakdown in stroke. *Neuron* 2014;**82**:603−17.
63. Yang GZ, Liu Y, Wang HF, Wilson R, Hui Y, Yu L, et al. Bioinspired core-shell nanoparticles for hydrophobic drug delivery. *Angew Chem Int Ed* 2019;**58**:14357−64.
64. Liu B, Hu F, Zhang JF, Wang CL, Li LL. A biomimetic coordination nanoplatform for controlled encapsulation and delivery of drug–gene combinations. *Angew Chem Int Ed* 2019;**58**:8804−8.
65. Zhang XX, Angsantikul P, Ying M, Zhuang J, Zhang QZ, Wei XL, et al. Remote loading of small-molecule therapeutics into cholesterol-enriched cell-membrane-derived vesicles. *Angew Chem Int Ed* 2017; **56**:14075−9.
66. Lockman PR, Mittapalli RK, Taskar KS, Rudraraju V, Gril B, Bohn KA, et al. Heterogeneous blood–tumor barrier permeability determines drug efficacy in experimental brain metastases of breast cancer. *Clin Cancer Res* 2010;**16**:5664−78.
67. Zhang SQ, Deng G, Liu FY, Peng B, Bao YM, Du FY, et al. Auto-catalytic delivery of brain tumor-targeting, size-shrinkable nano-particles for treatment of breast cancer brain metastases. *Adv Funct Mater* 2020;**30**:1910651.